Random and Systematic Errors in Thermophysical Property Measurements

Philip T. Eubank, David Van Peursem, Yun-Peng Chao, and Deepak Gupta
Dept. of Chemical Engineering, Texas A&M University, College Station, TX 77843

General procedures are outlined for the simulation and propagation of random and systematic errors in thermophysical property experiments. Density second virial coefficients B(T) from sonic velocity and Joule-Thomson (J-T) experiments are examined for error propagation where the connecting thermodynamic identity is a differential equation with missing boundary conditions. A recent controversy is addressed concerning B(T) at subcritical temperatures for pure hydrocarbon gases from direct density measurements vs. new sonic velocity data. Sonic velocity results are more likely correct with adsorption errors causing the problem in the density measurements.

Two new model consistency tests are developed for checking assumed temperature models in the reduction of sonic velocity and J-T data to B(T). Excellent values of B(T) are then obtained from either type of data when the original experiments are free of errors. Random errors propagate systematically when the connecting equation is a differential equation. Sonic data must be of high precision (± 10 ppm) to generate B(T) to ± 1 cm^3/mol due to complications in data reduction arising from the temperature model/random error interaction. Except perhaps for adsorption errors, systematic errors in the sonic velocities are unimportant to B(T). J-T data provide propagation factors near unity with errors in B(T) higher at higher temperature, unlike sonic velocities.

Introduction

In thermophysical property measurements, it is not uncommon for the measurements of one laboratory to exhibit pronounced systematic deviations from those of a second laboratory over a wide range of temperature and/or pressure. When the precision (reproducibility) of each data set is very high, then the disagreement can be ascribed to important systematic errors in either one data set or both. An example is the vapor pressure of methyl chloride from 313 to 408 K (Mansoorian et al., 1981) where careful, precise measurements of ± 1 kPa from two laboratories provided a systematic bias of about 30 kPa that was resolved only later when measurements from a third laboratory were published (Holldorff and Knapp, 1988).

One of the beauties of thermodynamics is its many connecting identities that allow calculation of one thermophysical property from measurements of a second property. Here we examine the density second virial coefficient $B(T)$:

$$(PV/RT) = Z = 1 + (B/V) + (C/V^2) + \ldots \qquad (1)$$

which can be extracted from independent measurement of gas densities, speeds of sound, and Joule-Thomson coefficients, among others, for pure components and excess enthalpies and liquid solubilities in gases for cross second virial coefficients, B_{12}. The very different random and systematic errors in these various experiments create a situation where $B(T)$ agreement, between two laboratories employing different measurements, strongly implies that the values are correct. However, disagreement demands examination of the random and systematic errors in the original data and how they propagate through the data reduction program into $B(T)$. Computer simulation of a particular experiment allows errors superimposed upon

Correspondence concerning this article should be addressed to P. T. Eubank.

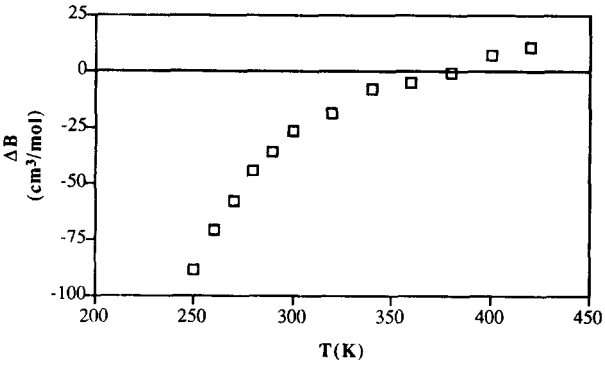

Figure 1. Deviations $\Delta B = B(T) - B$ (sonic).

$B(T)$ is from Dymond and Smith (1980), based upon selected P-V-T data, and B (sonic) is from Ewing et al. (1988).

the measured property to be traced through data reduction and into $B(T)$.

Some literature computer simulations exist for $B(T)$ from gas densities, particularly in regard to systematic adsorption errors that often plague these measurements at subcritical temperatures. Hall and Eubank (1972) superimposed Langmuir adsorption isotherms onto a Dieterici gas to show that adsorption errors accumulate in the Burnett experiment but not in the Burnett-Isochoric experiments. Later computer simulations (Kerns and Eubank, 1973; Eubank et al., 1988, 1990) have led to both new diagnostic and adsorption correction methods for density data from the Beattie, Burnett, and Burnett-Isochoric experiments. One particularly basic result is obvious from Eq. 1: errors in $B(T)$, e_B, are of the same order as those in $|Z-1|$, ignoring third virial effects. We may be able to measure Z to $\pm 0.01\%$, for a nonadsorbing gas, but as the subcritical temperature is lowered so is the vapor pressure causing Z of the saturated vapor to approach unity. For example with steam, $Z_v^\sigma = 0.9843$ at 373.15 K, so if $e_Z = 0.0001$, the fractional error in $|Z-1|$ is (1/157), as it is in $B(T)$. The error in Z has propagated from (1/10,000) to (1/157) or the propagation factor is about 64 from Z to B. Of course, steam is very adsorbing gas. For n-butane also at its NBP (272.67 K), $Z_v^\sigma = 0.9558$ providing a propagation factor (PF) of 24 so $B(T)$ should be more accurate because the PF is lower and the actual errors in $Z(1 > Z > Z_v^\sigma)$ should be less due to less adsorption. This example demonstrates that there are no truly direct methods for measurement of $B(T)$ and methods other than gas density should be considered for low reduced temperatures ($T_r < 0.8$).

Recent speed of sound measurements by Ewing et al. for the C_1-C_5 alkane hydrocarbon gases (neo-pentane: Ewing et al., 1987; n-butane: Ewing et al., 1988; n-pentane: Ewing et al., 1989; isobutane: Ewing and Goodwin, 1991; isopentane: Ewing and Goodwin, 1992a; methane: Ewing and Goodwin, 1992b; Trusler and Zarari, 1992a; ethane and propane: as cited by Boyes et al., 1992a) above 250 K have resulted in substantially less negative values of $B(T)$ for the butanes and pentanes from about 250–350 K. Figure 1 is a difference graph for n-butane illustrating the systematic deviation between sound speed and gas density (Dymond and Smith, 1980) derived $B(T)$. Ewing et al. attribute these differences to adsorption errors in the gas densities; few P-V-T experimentalists believe that adsorption is sufficiently high in hydrocarbon gases to cause

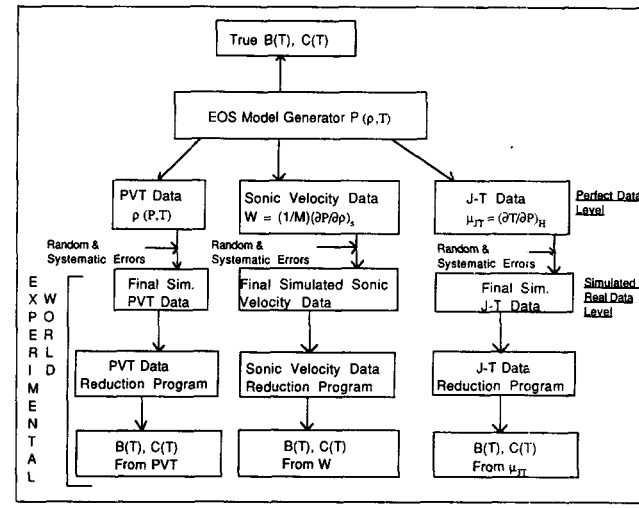

Figure 2. Simulations of thermophysical experiments which provide virial coefficients (pure gases).

errors in $B(T)$ of this order. Further, they doubt the credibility of $B(T)$ from sound speeds W because the connecting thermodynamic identity is a second-order differential equation with missing boundary conditions. However, recent advances in sound speed measurements, using spherical resonators, have improved the reproducibility of $W^2(P,T)$ to the order of 5-20 ppm. The present study was begun to provide PF for $W^2(P,T) - B(T)$ for various types of errors in W^2, develop consistency tests to ensure that the $B(T)$ results are internally consistent with boundary condition (or model) assumptions in the data reduction and, in general, resolve conflicts in $B(T)$ from these two important measurements.

Finally, the simulation methods developed here can be applied to any thermophysical property derived from any type of original measurements including the case where the connecting thermodynamic identity is a differential equation. It is clear that we should not initiate construction of experimental apparatus before such computer simulation of both our proposed apparatus and alternative apparatus. This ensures that the particular thermophysical property will be found to the desired accuracy level by the optimum apparatus considering apparatus simplicity, and time of construction, expense, speed of data procurement, and random and systematic errors in the original measurements.

Simulation Procedure

The rationale for the computer simulation of any experiment is shown in Figure 2, which is specifically drawn for virial coefficients from gas density, sonic velocity, and Joule-Thomson data. First, an equation-of-state (EOS) model generates error-free data for each experiment over a range of pressure and temperature. These data can be passed directly through the respective data reduction program, which uses the connecting thermodynamic identities, to calculate virial coefficients for comparison to the true EOS model values. The agreement may not be exact due to numerical errors in data reduction (for example, round-off errors) and, more importantly, assumptions made in data reduction to evaluate unknown boundary conditions when the connecting identity is a

differential equation. This second problem exists when sonic velocity and J-T data are used to evaluate density virial coefficients.

Next, random and/or systematic errors can be superimposed onto the error-free data and the resulting final simulated data again sent through data reduction. The propagation of these errors into the virial coefficients can then be found by comparison to the true model values. Unlike real experiments, simulations have the advantage that the correct final results are known. The EOS model needs but to roughly mimic the real world because we only compare it unto itself in simulations. It is the changes in the virial coefficients that are important rather than the exact values themselves. In this initial article, we only examine $B(T)$ from sonic velocity and J-T data.

Random errors (RE) are produced by a random number generator which yields Gaussian random number deviates (RND) of unit variance. These deviates are then scaled according to the amount of error under investigation. For example, if one wishes to induce a five parts per million (5 ppm) error onto the error-free (EF) variable X, the resulting equation is:

$$X_{RE} = X_{EF}[1 + \delta_{RE}(RND)] \tag{2}$$

with the scaling factor δ_{RE} being 5×10^{-6}. This results in X_{RE} having a random error variance of five ppm.

Three types of systematic errors were investigated in this work: fixed absolute errors (FAE), fixed fractional errors (FFE), and variable errors to mimic physical adsorption. FAE and FFE can be positive or negative in nature. A fixed absolute systematic error is introduced simply as:

$$X_{FAE} = X_{EF} \pm \delta_{FAE} \tag{3}$$

where δ_{FAE} is the amount of error under consideration. Likewise, a FFE is introduced as:

$$X_{FFE} = X_{EF}(1 \pm \delta_{FFE}) \tag{4}$$

where δ_{FFE} is the fractional amount of error under consideration. Real systematic errors are often of the FAE or FFE form over wide ranges of pressure and temperature. Other systematic errors, such as those caused by physical adsorption, vary widely with pressure and temperature. Adsorption increases with pressure along isotherms and rises nearly exponentially with falling temperature along isobars. Thus, a linear adsorption model may provide errors of the simple form:

$$(X_{AD} - X_{EF}) = C_0 P \exp(C_1/T) \tag{5}$$

where C_0 and C_1 are arbitrary constants indicative of the error level and its temperature sensitivity, respectively.

The propagation factor (PF), discussed in the introduction, is now formally defined as:

$$PF(T) = \left| \frac{(B_{ERROR} - B_{EF})/B_{EF}}{(W^2_{ERROR} - W^2_{EF})/W^2_{EF}} \right| \tag{6}$$

for sonic speeds and likewise for the Joule-Thomson experiment by replacing W^2 by μ_{JT}. This definition is based upon propagation of fractional errors, whereas, in some cases (for example, $B_{EF} \equiv 0$), it may be more meaningful to use the propagation of absolute errors which, however, carry units.

The Redlich-Kwong equation of state (R-K/EOS):

$$P = \frac{RT\rho}{1 - b\rho} - \frac{a\rho^2}{\sqrt{T}(1 + b\rho)}, \tag{7}$$

which provides

$$B_{RK}(T) = b - \frac{a}{RT^{1.5}}, \tag{8}$$

was selected for the gas density model. When the R-K constants are determined from the well-known critical constraints:

$$a = 0.427848 \frac{R^2 T_c^{2.5}}{P_c} \tag{9}$$

and

$$b = 0.08664 \frac{RT_c}{P_c}, \tag{10}$$

the reduced second virial coefficient, (BP_c/RT_c), is (-0.34084) at the critical temperature in agreement with experimental values of -0.34 ± 0.01 for all compounds from inert gases to steam. For subcritical temperatures, R-K generally predicts $B(T)$ too positive, even for nonpolar gases. However when simplicity is considered, R-K is likely the optimum EOS for simulations aimed at $B(T)$.

We further chose to simulate n-butane and use the following physical constants: $R = 8.3144$ cm^3-bar/mol-K, $M = 58.124$, $T_c = 452.2$ K, $P_c = 38.0$ bar, $b = 80.6$ cm^3/mol, and $a = 2.9 \times 10^8$ bar$\cdot$cm$^6\cdot\sqrt{\text{K}}$/mol^2. The isobaric ideal-gas-state heat capacity for n-butane was determined by:

$$(C_p^*/R) = 1.935 + 36.915 \times 10^{-3}(T/\text{K}) - 11.402 \times 10^{-6}(T/\text{K})^2 \tag{11}$$

This equation (Smith and Van Ness, 1987) was chosen for its simplicity and because the values agree closely with the more precise correlation of Chen et al. (1975) over the temperature range 250 to 420 K, corresponding to the sound speed measurements of Ewing et al. (1988).

Error-free sound speeds $W(P,T)$ can then be generated from the identity:

$$MW^2 = \left(\frac{\partial P}{\partial \rho}\right)_T + (T/\rho^2)\left(\frac{\partial P}{\partial T}\right)_\rho^2 \left[C_v^* - T \int_0^\rho \left(\frac{\partial^2 P}{\partial T^2}\right)_\rho \frac{1}{\rho^2}\, d\rho \right]^{-1} \tag{12}$$

where $C_v^* = (C_p^* - R)$. Likewise, the Joule-Thomson coefficient $\mu_{JT}(P,T)$ can be found from:

$$\mu_{JT} \equiv (\partial T/\partial P)_H$$

$$= \frac{T(\partial P/\partial T)_\rho - \rho(\partial P/\partial \rho)_T}{T(\partial P/\partial T)_\rho^2 + \rho^2(\partial P/\partial \rho)_T\left[C_v^* - T\int_0^\rho \left(\frac{\partial^2 P}{\partial T^2}\right)_\rho \frac{1}{\rho^2}\, d\rho\right]} \quad (13)$$

Data Reduction

Sound speeds

The simulated sonic speeds were first analyzed on isotherms to obtain the acoustic virial coefficients:

$$W^2 = W_o^2\left(1 + \frac{\beta_a}{RT}P + \frac{\gamma_a}{RT}P^2 + \ldots\right) \quad (14)$$

where β_a and γ_a are the acoustic second and third virial coefficients, respectively, and W_o^2 is defined by:

$$W_o^2 = \frac{RT\gamma^*}{M} \quad (15)$$

where

$$\gamma^* = \frac{C_p^*}{C_v^*} \quad (16)$$

The acoustic second virial coefficient can be defined explicitly by rearranging Eq. 14 and taking the zero-pressure limit:

$$\beta_a = \lim_{P\to 0}\left\{\frac{[(W/W_o)^2 - 1]RT}{P}\right\} \quad (17)$$

Thus, β_a is simply the zero-pressure intercept on the plot of $[(W/W_o)^2 - 1]\ RT/P$ vs. P. The acoustic second virial coefficient is related to the density second virial coefficient and its two higher temperature derivatives by the thermodynamic identity:

$$F(T) \equiv \frac{\beta_a}{2} = B + (\gamma^* - 1)T\frac{dB}{dT} + \frac{(\gamma^* - 1)^2T^2}{2\gamma^*}\frac{d^2B}{dT^2} \quad (18)$$

Van Dael (1975) has discussed the history of this equation. Generally, a functional form of $B(T)$ is assumed and the constants evaluated from measurements of β_a over a wide temperature range. A second procedure is to accept values of $B(T)$ at two different temperatures from gas density measurements and numerically integrate Eq. 18. Trusler and Zarari (1992b) have recently described such a procedure but conclude that it is not accurate for integration from high temperatures ($T_r > 1$), where the gas density values contain no adsorption errors, to lower temperatures where the derivative terms of Eq. 18 become more important. The present work uses the conventional procedure of assuming a $B(T)$ form.

Table 1 lists the twelve temperature forms used here for both sonic speeds and J-T data. Of course, the third form is "correct" as it agrees with that of a R-K EOS. However, one of our several objectives is to study the effect of selecting various "wrong" forms upon the final $B(T)$. We must now pretend to be a sonic velocity experimentalist who has just measured

Table 1. Assumed Temperature-Dependent Forms for the Density Second Virial Coefficient

Model	Temperature Form
1	$B = \beta_0 + \beta_1 T^{-0.5}$
2	$B = \beta_0 + \beta_1 T^{-1}$
3	$B = \beta_0 + \beta_1 T^{-1.5}$
4	$B = \beta_0 + \beta_1 T^{-2}$
5	$B = \beta_0 + \beta_1 T^{-2.5}$
6	$B = \beta_0 + \beta_1 T^{-1} + \beta_2 T^{-1.5} + \beta_3 T^{-2}$
7	$B = \beta_0 + \beta_1 T^{-1} + \beta_2 T^{-1.5}$
8	$B = \beta_0 + \beta_1 T^{-1.5} + \beta_2 T^{-2}$
9	$B = \beta_0 + \beta_1 T^{-0.5} + \beta_2 T^{-1}$
10	$B = \beta_0 + \beta_1 T^{-1} + \beta_2 T^{-2}$
11	$B = \beta_0 + \beta_1 \exp(\beta_2 T^{-1})$
12*	$B = \frac{\beta_1}{n}\sum_{j=0}^{\infty}\frac{\Gamma\left(\frac{6j-3}{n}\right)}{j!}\left\{\frac{n^{1/n-6}}{[6^{6/n-6}(n-6)\beta_2 T]^{1/n}}\right\}^{j(n-6)+3}$

* Where n is from the Lennard-Jones potential (see Maitland et al., 1981).

$W^2(P,T)$, corresponding to the simulated real data level of Figure 2. To find $B(T)$, the experimentalist must select a temperature form (Table 1) but *without our prior knowledge of which form is more nearly correct*, that is, consistent with the $W^2(P,T)$ measurements. Because we "know all the answers" in simulation, new self-consistency tests can be developed from our results to aid experimentalists in future reduction of sonic data to $B(T)$. It is important to understand that in reducing real sonic velocity data the "correct form" of $B(T)$ cannot be found *a priori*. The data reduction may later provide a form consistent with the original $W^2(P,T)$ measurements but such a form should be regarded as only approximate to the true $B(T)$ and may not be unique, mathematically.

When the R-K temperature form, Eq. 8, is used with the connecting identity of Eq. 18, there results:

$$F_{RK}(T) = b - \frac{a}{RT^{1.5}}\left[1 - \frac{3(\gamma^* - 1)}{2} + \frac{15(\gamma^* - 1)^2}{8\gamma^*}\right] \quad (19)$$

Values of $F(T)$ generated for a R-K gas with no superimposed errors should agree closely with those from this equation. Table 2 shows this agreement.

Joule-Thomson coefficients

Simulation of the second virial coefficient from Joule-Thomson data starts by applying the real-gas inverse volume power series (Maitland et al., 1981):

$$\mu_{JT} = -\left[B - T\frac{dB}{dT}\right] + \left[2B^2 - 2TB\frac{dB}{dT} - 2C + T\frac{dC}{dT} - \frac{RT^2}{C_p^*}\left(B - T\frac{dB}{dT}\right)\frac{d^2B}{dT^2}\right]\frac{1}{V} + \ldots \quad (20)$$

where C is the density third virial coefficient and V the molar volume. A functionality explicit in $B(T)$ and its first derivative can be determined by simply taking the limit of Eq. 20 as $P \to 0$, which is equivalent to $V \to \infty$. This is accomplished graphically by plotting $\mu_{JT}C_p$ vs. P and taking the zero-pressure intercept. The result is redefined as:

Table 2. Comparison of Simulated Values of $F(T)$ and $F_{RK}(T)$

T/K	$F(T)$	$F_{RK}(T)$	γ^*	T/K	$F(T)$	$F_{RK}(T)$	γ^*
250	−678.264	−678.273	1.1058	360	−375.280	−375.280	1.0785
270	−601.506	−601.509	1.0993	390	−326.469	−326.469	1.0735
300	−508.372	−508.372	1.0910	420	−285.800	−285.800	1.0693
330	−434.725	−434.725	1.0842				

$$G(T) \equiv \lim_{P\to 0} (\mu_{JT} C_p) = \lim_{P\to 0} (-\partial H/\partial P)_T$$

$$= \left[B - T\frac{dB}{dT} \right] = T^2 \left[\frac{d(B/T)}{dT} \right] \quad (21)$$

The next step in the data reduction scheme is to assume a temperature form for $B(T)$. The same temperature dependent forms as used for the sound speeds, Table 1, will also be applied for Joule-Thomson coefficient data. With the temperature form chosen, a least-squares linear regression is performed on Eq. 21 to determine the best set of constants. The results are then compared with the true temperature form, Eq. 4, to determine the Joule-Thomson propagation factor (PF) as in Eq. 6. Analogous to Eq. 19:

$$G_{RK}(T) = -b + (5/2)(a/RT^{1.5}) \quad (22)$$

Again, we simulate *n*-butane over the same range of pressure and temperatures as for the sound speeds. Like the sound speeds, the error-free values of $\mu_{JT}(P,T)$ for the R-K gas are in rough agreement with experiment (see Kennedy et al. (1936) for μ_{JT} data covering part of the present temperature/pressure range). While such comparisons are made by Van Peursem (1991), they are not presented here because close agreement is not necessary for validity of the error propagation results to follow which compares simulation to simulation, as discussed previously.

Results Including New Model Consistency Tests

Sound speeds

This section examines results from simulated data that are free of errors, contain superimposed random errors, contain one of three different types of imposed systematic errors, or contain a combination of these errors. New model consistency tests are presented as they were developed logically to analyze the above data sets.

Error-Free Simulations. Table 3 provides the results for the various temperatures forms of Table 1 for comparison to the correct R-K values of $B(T)$. As expected, model 3, as well as other forms containing the $T^{-3/2}$ term (models 6, 7 and 8), reproduced the R-K values with little numeric error. Models 9–12 provide small errors of a few cm^3/g-mol at the lowest temperature, whereas the remaining models fail. Models 11 and 12 (exponential and Lennard-Jones, respectively) are often used by modern sonic velocity experimentalists.

Our original model consistency test (MCT), which was first proposed by Chao (1990), is here termed the first-order MCT or MCT-1. Equation 18 is rearranged to form $[F(T)\text{-}B]$ as the numerator on the LHS of the MCT-1 test equation with the RHS containing only simple functions of temperature. For example, temperature models 1–5 provide:

$$\ln\left\{ \frac{F(T)-B}{\beta_1 k_i(\gamma^*-1)\left[1+\dfrac{(k_i-1)(\gamma^*-1)}{2\gamma^*}\right]} \right\} \equiv \ln(Q_i) = k_i \ln(T) \quad (23)$$

for the form $B = \beta_o + \beta_1 T^{k_i}$. Values of $B(T)$ from the data reduction program (Table 3) are tested for internal consistency with the $F(T)$ measurements by plotting $\ln(Q_i)$ vs. $\ln(T)$. If the resultant graph is nonlinear, the assumed temperature model is deemed inconsistent and rejected. Figures 3a and 3b result from Table 3 and Eq. 23 for model 2 (for simple cubic EOS other than R-K) and model 3 (R-K form), respectively. Van Peursem (1991) provides equations analogous to Eq. 23 for the remaining temperature models (6–12). Here we list only the MCT-1 equation for the exponential model 11, because it

Table 3. Comparison of Error-Free Second Virial Coefficients from Sound Speeds*

		Models											
T/K	RK	1	2	3	4	5	6	7	8	9	10	11	12
250	801.53	754.75	777.52	801.53	826.68	852.86	801.51	801.52	801.52	799.54	802.53	803.56	803.55
270	705.36	683.12	694.28	705.35	716.20	726.69	705.35	705.35	705.35	704.89	705.54	705.68	705.64
300	590.46	589.41	590.23	590.46	590.06	588.99	590.46	590.46	590.46	590.73	590.30	590.11	590.09
330	501.06	508.78	505.09	501.06	496.72	492.11	501.06	501.06	501.06	501.28	500.96	500.86	500.87
360	429.89	438.46	434.15	429.89	425.73	421.72	429.89	429.89	429.89	429.86	429.92	429.96	429.96
390	372.14	376.42	374.12	372.14	370.49	369.18	372.14	372.14	372.14	371.97	372.22	372.31	372.31
420	324.51	321.15	322.66	324.51	326.65	329.07	324.51	324.51	324.51	324.44	324.53	324.55	324.55
RMSE**	*****	16.220	8.2329	0.0032	8.4334	17.026	0.0069	0.0051	0.0053	0.5829	0.2895	0.5815	0.5777

*Second virial coefficients are negative with units of cm^3/mol.
**Root mean square error between RK and the respective model for 18 temperatures between 250 and 420 K at 10° intervals.

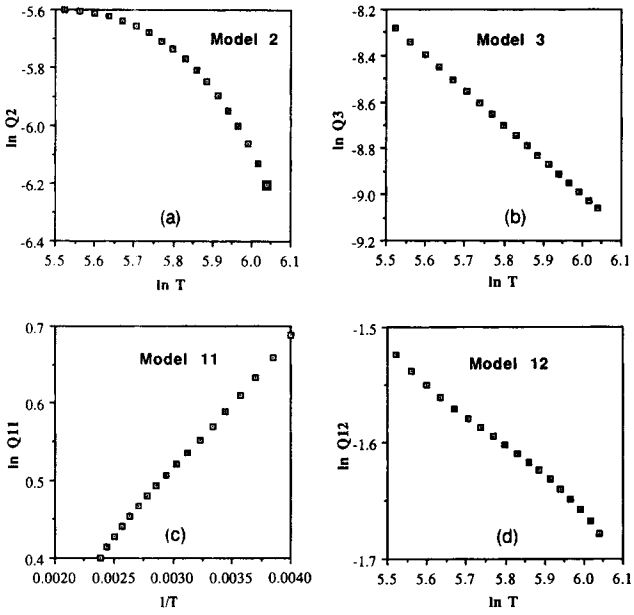

Figure 3. First-order model consistency test with error-free data.

has been used in the many previously referenced publications of Ewing et al.:

$$\ln\left\{\frac{F(T)-B}{\beta_1\beta_2 T^{-1}(\gamma^*-1)\left[\dfrac{(\beta_2 T^{-1}+2)(\gamma^*-1)}{2\gamma^*}-1\right]}\right\} \equiv \ln(Q_{11}) = \beta_2 T^{-1} \quad (24)$$

Figures 3c and 3d for models 11 and 12, respectively, provide only slight nonlinearity. Thus, the exponential and L-J models are judged to pass MCT-1.

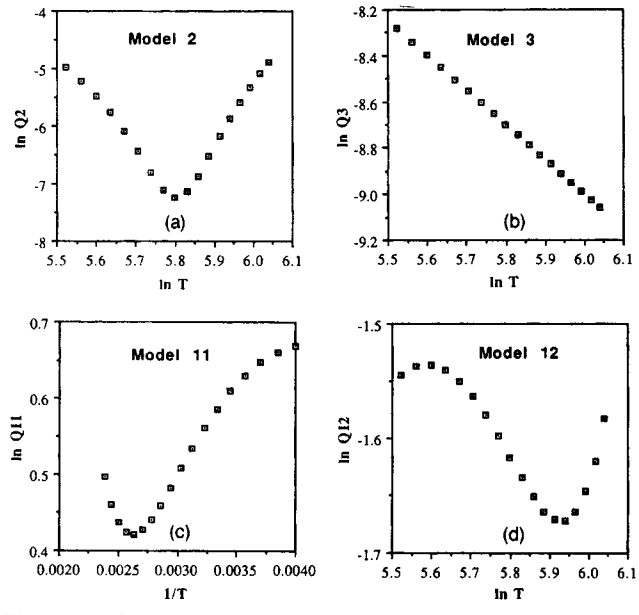

Figure 4. Second-order model consistency test with error-free data.

The second consistency test (MCT-2), as developed by Van Peursem (1991), takes the MCT-1 one step further by checking, in effect, consistency of (d^2B/dT^2) rather than (dB/dT). Here Eq. 18 is rearranged to form $[F(T)-B-(\gamma^*-1)T(dB/dT)]$ as the numerator on the lefthand side of the MCT-2 test equation with the RHS again a simple function of temperature. Models 1-5 then provide:

$$\ln\left\{\frac{F(T)-B-(\gamma^*-1)T\dfrac{dB}{dT}}{\dfrac{\beta_1 k_i(k_i-1)(\gamma^*-1)^2}{2\gamma^*}}\right\} \equiv \ln(Q_i) = k_i \ln(T) \quad (25)$$

Values of both B and (dB/dT) are from the model with corresponding constants (β_0 and β_1, and so on) from the regression routine of the data reduction program using Eq. 18. Figures 4a and 4b result from Table 3 and Eq. 25 for models 2 and 3, respectively. Again, Van Peursem (1991) provides equations analogous to Eq. 25 for models 6-12, and here we list only the MCT-2 equation for model 11:

$$\ln\left\{\frac{[F(T)-B-(\gamma^*-1)T(dB/dT)]}{\beta_1\beta_2 T^{-1}(\beta_2 T^{-1}+2)(\gamma^*-1)^2/2\gamma^*}\right\} \equiv \ln(Q_{11}) = \beta_2 T^{-1} \quad (26)$$

Figures 4c and 4d for models 11 and 12, respectively, show pronounced deviation from linearity. MCT-2 is thus more sensitive to the temperature model than is MCT-1.

Simulations with Random Errors. Random errors were imposed upon the error-free values of W^2 at levels of 5 ppm and 50 ppm (see Eq. 2). The lower level is that claimed by Ewing whereas the higher level is more realistic when using older sonic velocity measurements. Virtually all the results of this article can be scaled linearly; that is, the resultant errors in $B(T)$ at the 50 ppm level are nearly ten times those at the 5 ppm level. We generally report the results at the higher level in order to detect a significant change in $B(T)$; experimentalists can estimate the errors in their original measurements and scale accordingly.

Two important results were discovered during the analysis of random errors. First, *random errors in $W^2(P,T)$ propagate systematically into $B(T)$* due to the required assumption of a temperature model for $B(T)$ in the connecting identity, Eq. 18. Normally, random errors propagate randomly when the connecting identity does not involve derivatives. Secondly, it is not enough to fix the random error level but further consideration must be given to the dominant outliers superimposed upon W^2(EF), as in Eq. 2. The random number deviates (RND) are additionally important as to both their magnitude and sign. While this second effect is present in any statistical analysis of random errors, it appears to be magnified by having a second-order differential equation as the connecting identity. As a yardstick of this second effect, the square mean (SM) is defined from the RDN as:

$$\text{Square Mean} \equiv \frac{\sqrt{\sum_{i=1}^{n^+}(\text{RND}_i^+)^2}}{n^+} - \frac{\sqrt{\sum_{j=1}^{n^-}(\text{RND}_j^-)^2}}{n^-} \quad (27)$$

Table 4. Statistical Data for Four Random Error Simulations of Sound Speed

Simulation	1(LPM-5)	2(HNM-5)	3(LNM-50)	4(HPM-50)
Number of Points	360	360	360	360
Square Mean	−0.005684	−0.010700	−0.002061	0.008228
Mean	0.001054	−0.155934	−0.003237	0.124787
Variance	0.834539	1.038859	0.951315	0.974008
Standard Deviation	0.913531	1.019244	0.975354	0.986919
Absolute Deviation	0.735190	0.815380	0.776969	0.778878
Skewness	−0.035576	−0.146515	−0.036016	−0.008052
Kurtosis	−0.302221	0.051521	0.474806	0.260852

Note: Each Datum is for the RND of Eq. 2.

where RND^+ and RND^- are the positive and negative RND, respectively. The square mean statistic is an attempt to determine the magnitude and direction of the outlier effect when there are a total of n^+ positive random errors superimposed upon $W^2(P,T)$ and n^- negative errors.

We present here the results for four simulations: a low positive mean (LPM) of the RND at the 5 ppm level, a high negative mean (HNM) at 5 ppm, a low negative mean (LNM) at 50 ppm, and a high positive mean (HPM) at 50 ppm. Table 4 provides usual statistical information plus the square mean (Eq. 27) for these independent, random error generations. For the same error level, two simulations correspond to repeating a complete set of $W^2(P,T)$ data in the laboratory. *Analysis of a single simulation often provides misleading conclusions.* Random simulations in addition to the four cited here have been done by Chao (1990) and by Van Peursem (1991); while our conclusions agree with results presented here, they are also based upon these addition simulations (roll of the die).

Table 5 shows how these random errors propagate into $B(T)$ depending upon the temperature model assumed. Only results for the lowest and highest temperatures are given along with the root mean square error from R-K for all of the 18 temperatures of Table 3. First, when the R-K temperature model is chosen, the four simulations result in propagation factors (PF) of Eq. 6 of 45, 227, 54, and 112, respectively, at 250 K and 12, 80, 17, and 54, respectively, at 420 K. A good average PF is 100 at 250 K and 30 at 420 K, but these values can be two to three times higher when a few dominant outliers are present whereas they may be two to three times lower when the outliers are absent.

Models 6–8 containing the R-K form perform about the same as model 3. Models 1, 2, 4, and 5 continue to yield poor results as with the error-free speed sounds of Table 3. However, models 9–12, which gave $B(T)$ within a few cm^3/mol with error-free data, now yield more erratic results. The average PF for these latter four temperature models are 480, 445, 444, and 63, respectively, for the four simulations of Table 5 at 250 K whereas the corresponding values at 420 K are 34, 111, 56, and 60. The outlier effects appear masked by the interaction of temperature model error with random error. The PF are generally more sensitive to temperature with the HPM-50 simulation an exception.

Models 9–12 are important because they likely represent the small temperature model errors present in the reduction of real

Table 5. Comparison of Density Second Virial Coefficient ($-B/cm^3 \cdot mol^{-1}$) with Random Errors in Sound Speeds

		Temperature Model											
T/K	RK	1	2	3	4	5	6	7	8	9	10	11	12
						Simulation 1 (LPM-5)							
250	801.53	754.58	777.35	801.35	826.50	852.68	803.24	801.68	801.74	799.64	802.72	803.82	803.85
420	324.51	321.14	322.65	324.49	326.63	329.05	324.56	324.52	324.52	324.45	324.55	324.57	324.57
RMSE*	****	16.273	8.2867	0.0960	8.3805	16.974	0.5086	0.0965	0.1091	0.5521	0.3632	0.6709	0.6775
						Simulation 2 (HNM-5)							
250	801.53	755.58	778.39	802.44	827.64	853.86	799.85	801.80	801.70	799.91	802.76	803.70	803.64
420	324.51	321.01	322.53	324.38	326.53	328.96	324.27	324.32	324.32	324.27	324.34	324.36	324.35
RMSE*	****	15.933	7.9389	0.4363	8.7576	17.356	0.6059	0.3210	0.3160	0.5883	0.4548	0.6625	0.6409
						Simulation 3 (LNM-50)							
250	801.53	756.28	779.35	803.70	829.22	855.80	803.34	817.81	818.68	814.95	819.28	821.33	821.70
420	324.51	321.02	322.46	324.23	326.31	328.68	325.04	325.41	325.41	325.33	325.44	325.44	325.44
RMSE*	****	15.713	7.6416	1.0461	9.3168	18.017	2.9749	5.6166	5.8017	4.9291	5.9668	6.4052	6.4697
						Simulation 4 (HPM-50)							
250	801.53	750.78	773.31	797.06	821.95	847.86	794.53	798.20	798.21	796.24	799.21	800.26	800.27
420	324.51	322.08	323.57	325.38	327.50	329.89	325.38	325.48	325.47	325.42	325.50	325.51	325.51
RMSE*	****	17.679	9.7991	2.0970	6.9997	15.447	2.4999	1.8322	1.8374	2.1638	1.7235	1.6836	1.6985

*RMSE is the root mean square error of the model result from RK for 18 temperatures between 250 and 420 K at 10° intervals.

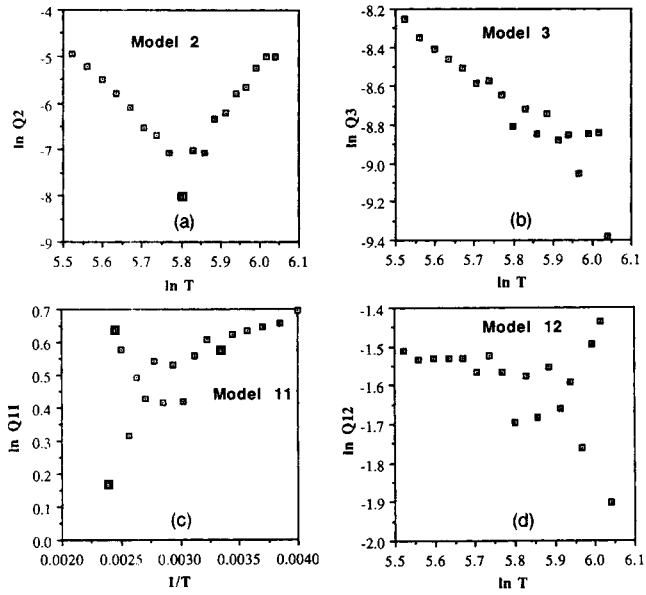

Figure 5. Second-order model consistency test with random errors (5 ppm LPM).

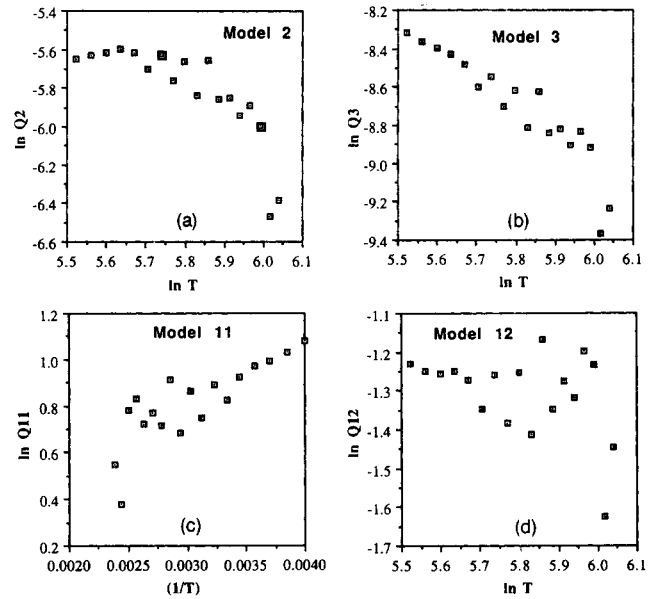

Figure 7. First-order model consistency test with random errors (50 ppm LNM).

sound speed data. Indeed, with error-free data, these errors can only be discerned with MCT-2. How is the selection of a good temperature model affected by the presence of random errors? To gain insight to this difficult question, we examined the results of the MCT; Van Peursem (1991) found that the sensitivity of MCT-2 was necessary at the 5 ppm level whereas this test was too sensitive at the 50 ppm level, resulting in such strong scatter on the diagrams that the consistency test for linearity was meaningless even for model 3. Thus, MCT-1 was found more useful at 50 ppm.

Figures 5a–5d show the MCT-2 diagrams for temperature models 2, 3, 11, and 12, respectively, for the first random simulation (LPM-5), which has few outliers. While model 2 can be discarded, comparison of Figures 5c and 5d with 4c and 4d, respectively, show the linear test no longer conclusive for models 11 and 12. Is it random scatter or systematic deviation from linearity at the higher temperatures?

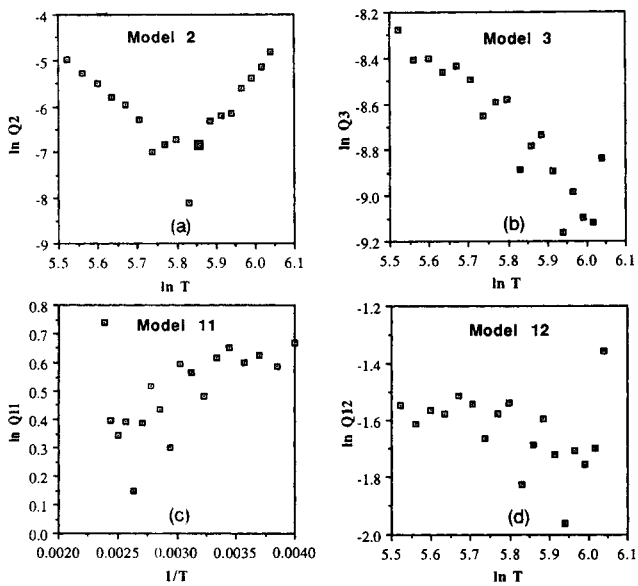

Figure 6. Second-order model consistency test with random errors (5 ppm HNM).

The second simulation (HNM-5), which does contain a number of dominant outliers, provides the corresponding diagrams of Figures 6a–d. Now the scatter for model 3 has worsened to the point where it appears no better than that for models 11 and 12. Indeed, Table 5 shows model 3 to yield only slightly better $B(T)$.

Figures 7a–7d for the third simulation (LNM-50) with MCT-1 show that we have nearly lost all ability to discern between a poor temperature model (2) and the correct model (3). The final $B(T)$ results of Table 5 are far superior for model 3 but the experimentalist would not know which temperature form to choose.

The fourth simulation (HPM-50) is perhaps the most interesting. Figure 8b (model 3) provides more consistency under MCT-1 than Figures 8c and 8d, but somewhat better final $B(T)$ results (Table 5) are obtained with the last two models.

Before proceeding to the simpler topic of systematic errors, some detailed conclusions concerning random errors are offered:

(1) Poor temperature models get little worse in $B(T)$ when large random errors are introduced whereas the better temperature models are adversely affected.

(2) A large number of random errors simulations are necessary to draw meaningful conclusions or, often, to see that there is no clear conclusion.

(3) Model 11 (exponential) provides nearly the same results as model 12 (Lennard-Jones) in all cases, and thus this simple model is preferable. Nature, of course, obeys none of these models in general. That model 11 does so well in treating data based upon an R-K gas indicates that the reverse would also be true. Any of the "reasonable" models (3, 6–12) are close enough to one another to provide similar $B(T)$ results for random simulations with high square means. Only high precision (5 ppm) simulations with low square means allow MCT

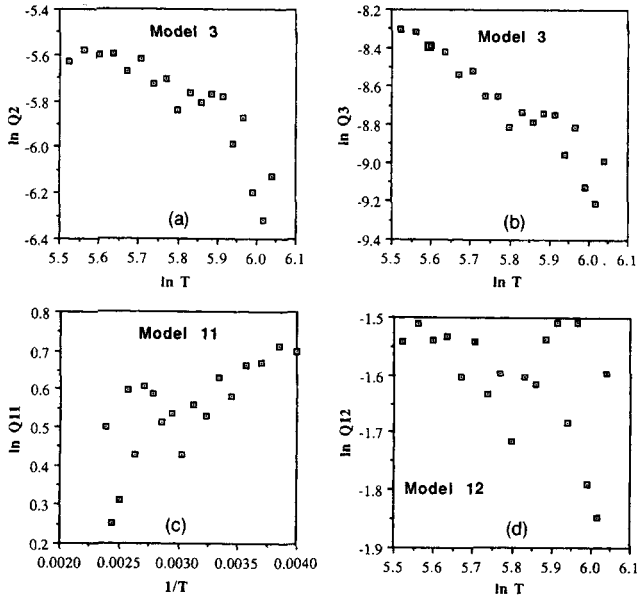

Figure 8. First-order model consistency test with random errors (50 ppm HPM).

to discern between these temperature forms. The importance of extremely high precision in sonic speed data is obvious.

Simulations with Systematic Errors. As noted previously, three types of systematic error were investigated: fixed absolute errors (FAE), fixed fractional errors (FFE), and variable errors to mimic physical adsorption. In each case, the error, from Eqs. 3-5, respectively, was superimposed upon the error-free

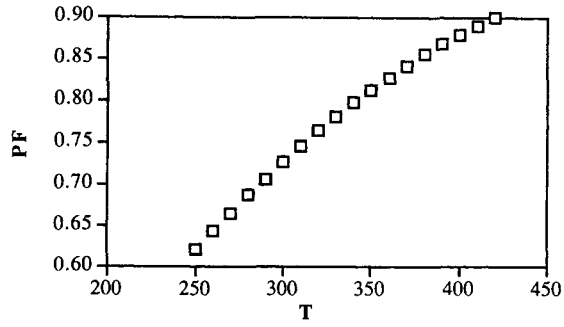

Figure 9a. Error propagation factor due to 50 ppm fixed absolute errors.

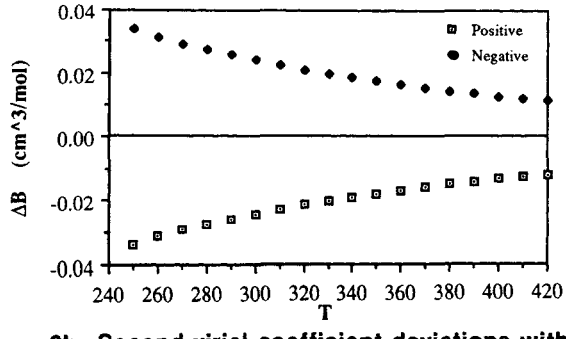

Figure 9b. Second virial coefficient deviations with 50 ppm fixed absolute errors.

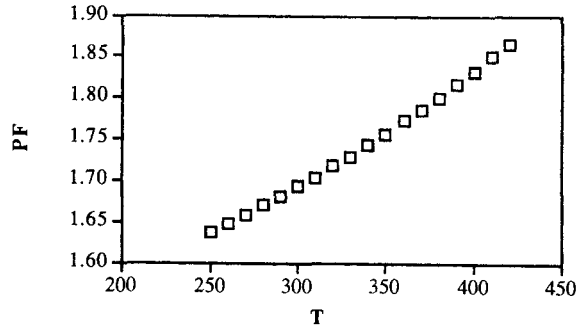

Figure 10a. Error propagation factor due to 50 ppm fixed fractional errors.

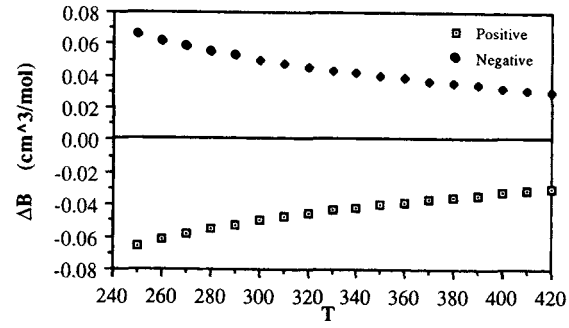

Figure 10b. Second virial coefficient deviations with 50 ppm fixed fractional errors.

value of $W^2(P,T)$, and the resultant data set reduced to $B(T)$ assuming a temperature form.

A positive 50 ppm FAE of 2.51 $(m/s)^2$ was added to each value of W^2. As seen from Eqs. 3 and 14, FAE do not change the slopes β_a or $F(T)$ but only only the intercept W_0^2 or γ^*. However, $B(T)$ is affected because both γ^* and $F(T)$ appear in Eq. 18. While secondary to $F(T)$, the effect of changing γ^* upon $B(T)$ is greater than expected because it appears as $(\gamma^* - 1)$ in Eq. 18 and γ^* is only 7-10% above unity (see Table 2). Figures 9a and 9b show the PF and error in $B(T)$ when temperature model 3 is used to reduce data with both a positive and negative FAE at the 50 ppm level. The very small PF and error in $B(T)$ show that even relatively large FAE cause little damage to $B(T)$. The root mean squared error in $B(T)$ for the present twelve temperature forms of Table 1 are, respectively: 16.214, 8.224, 0.022, 8.449, 17.045, 0.021, 0.021, 0.021, 0.572, 0.0302, 0.593, and 0.589. Further, the MCT-2 is able to select temperature model 3 similar to the error-free example of Figure 4.

Next, a positive FFE of 50 ppm (or $\delta_{FFE} = 50 \times 10^{-6}$) was superimposed upon $W_{EF}^2(P,T)$. Now both γ^* and $F(T)$ are altered. Figures 10a and 10b show that the PF and error in $B(T)$ are indeed increased over those for the FAE but they remain small. The root mean squared error in $B(T)$ for the 18 temperatures is 0.00470 (model 3), 0.5680 (model 11), and 0.5649 (model 12). Again, MCT-2 is able to select model 3.

Finally, adsorption-like errors given by Eq. 5 were superimposed upon $W_{EF}^2(P,T)$. The adsorption constants of Eq. 5 were set at $C_0 = 15.9168$ $(m/s)^2 \cdot Pa^{-1}$ and $C_1 = 2{,}339.37$ K corresponding to a 50 ppm error at (250 K, 1 bar) and a 25 ppm error at (270 K, 1 bar). The constant C_1 should be roughly

Table 6. Deviations of Density Second Virial Coefficients (ΔB, cm^3/mol) with Adsorption and Other Errors in Sound Speeds

	Temperature Model						
T/K	3	6	7	8	9	10	11
	Simulation 1 (Adsorption Only)						
250	−4.5167	−9.9263	−7.6102	−7.9272	−5.3099	−8.7941	−10.1832
270	−3.5808	−5.4487	−4.9938	−5.0675	−4.4500	−5.2296	−5.4221
300	−2.4627	−2.1158	−2.4720	−2.4301	−2.7842	−2.2919	−2.0433
330	−1.5927	−0.8208	−1.0566	−1.0212	−1.3066	−0.9352	−0.8001
360	−0.9001	−0.3956	−0.3445	−0.3427	−0.3193	−0.3681	−0.4083
390	−0.3381	−0.2761	−0.0888	−0.1074	0.0927	−0.1825	−0.2911
420	0.1254	−0.1925	−0.1330	−0.1437	−0.0596	−0.1640	−0.1926
RMSE*	1.7139	3.7533	2.8979	3.0038	2.1991	3.2889	3.7586
	Simulation 2 (Random, FAE, FFE; all 50 ppm)						
250	−4.3705	−6.8679	−3.2210	−3.2082	−1.2319	−4.2384	−5.2399
270	−3.3035	−3.4960	−2.7801	−2.7985	−2.2980	−2.9875	−3.1331
300	−2.0320	−1.4680	−2.0289	−2.0434	−2.2912	−1.8771	−1.7016
330	−1.0416	−0.8703	−1.2410	−1.2366	−1.4603	−1.1357	−1.0376
360	−0.2531	−0.5407	−0.4596	−0.4431	−0.4476	−0.4765	−0.5029
390	0.3867	−0.0011	0.2942	0.3082	0.4427	0.2165	0.1399
420	0.9144	0.9175	1.0108	1.0064	1.0766	0.9833	0.9620
RMSE*	1.9509	2.6373	1.5779	1.5820	1.5128	1.8261	2.1076
	Simulation 3 (Adsorption RE, FAE, FFE; all 50 ppm)						
250	−8.8863	−16.8034	−10.8351	−11.1397	−8.5220	−12.0217	−13.3770
270	−6.8849	−8.9463	−7.7747	−7.8668	−7.2063	−8.0216	−8.2292
300	−4.4940	−3.5815	−4.4994	−4.4719	−4.7993	−4.3255	−4.0943
330	−2.6337	−1.6889	−2.2956	−2.2557	−2.5525	−2.1715	−2.0356
360	−1.1527	−0.9353	−0.8025	−0.7842	−0.7951	−0.8184	−0.8456
390	0.0492	−0.2773	0.2060	0.2014	0.3731	0.1185	0.0217
420	1.0403	0.7243	0.8770	0.8619	0.9550	0.8439	0.8127
RMSE*	3.6650	6.2943	4.3711	4.4701	3.7236	4.7283	5.1471

*Root mean square error between RK and the respective model for 18 temperatures between 250 and 420 K at 10° intervals.

correct whereas the adsorption level C_0 is likely 10–100 times larger than in real sound speed experiment. Again, we have set the error level high to see an effect knowing the experimentalist can downscale the effect linearly. Adsorption causes decrease in the sonic speed (Mehl and Moldover, 1982) and being roughly linear with pressure, at these low pressures, causes $F(T)$ to be more negative and, hence, $B(T)$ is more negative. The effect upon the perfect gas state heat capacities and γ^* is slight but nonzero. Table 6 first shows the effect of this adsorption error alone upon $\Delta B \equiv (B - B_{RK})$ for seven temperature models at select temperatures. The root mean squared errors in Table 6 are, however, calculated for all 18 temperatures at 10 degree intervals. Adsorption can cause slight positive errors in $B(T)$ at the higher temperatures with these "better" models. The adsorption effect is significant even with model 3 and highly temperature dependent as expected. The second simulation of Table 6 is with a new random error generation (50 ppm). The effect of the FAE and FFE remains unimportant either individually or when present with other errors. Thus the errors of the second simulation are due almost entirely to the random errors. Comparison with Table 5 shows this RE generation similar to LNM-50 with dominant outliers. Combination of the first two simulations of Table 6 results in the third, which contains all the types of error used in this manuscript. The negative RE and adsorption errors are nearly additive from the first two simulations resulting in high deviations for $B(T)$. This simulation represents the ultimate worse scenarios for sound speed data. Addition of the first simulation ΔB of Table 6 to those of the various RE simulations of Table 5 illustrates that in some cases the adsorption and RE contributions to $B(T)$ compensate one another depending upon the temperature and model assumed.

Joule-Thomson coefficients

The results of this section follow those of the previous section for sound speeds and only differences in the results will be given here. Equations 13, 20, 21 and 22 are used in the R-K simulation; the J-T experimentalist must also possess independent $C_p^*(T)$ data, which is available for a wide variety of compounds.

Error-Free Simulations. Table 7 shows the high sensitivity to the temperature model at select temperatures with the root mean squared error again calculated for all 18 temperatures. Unlike sound speeds, the errors are generally worse at the highest temperatures.

Because Eq. 21 is of first order, only the MCT-1 can be applied resulting in:

$$\ln\left\{\frac{G(T)+B}{\beta_1 k_i}\right\} \equiv \ln(Q_i) = k_i \ln(T) \tag{28}$$

for models 1–5 and

$$\ln\left\{\frac{-T[G(T)+B]}{\beta_1\beta_2}\right\} \equiv \ln(Q_{11}) = \beta_2 T^{-1} \tag{29}$$

Table 7. Comparison of Error-Free Second Virial Coefficients for the J-T Experiment*

		Model											
T/K	RK	1	2	3	4	5	6	7	8	9	10	11	12
250	801.53	349.44	632.20	801.55	914.09	994.09	802.03	801.38	801.44	915.87	772.76	757.63	765.92
270	705.36	219.52	523.64	705.38	825.88	911.36	705.90	705.19	705.26	828.86	674.28	657.94	666.90
300	590.46	49.57	387.94	590.49	725.16	821.07	591.07	590.28	590.35	727.61	555.98	537.85	547.81
330	501.06	−96.64	276.91	501.10	650.64	757.54	501.73	500.87	500.94	651.91	463.14	443.20	454.15
360	429.89	−224.2	184.39	429.93	593.96	711.38	430.62	429.68	429.76	594.49	388.50	366.72	378.66
390	372.14	−336.7	106.10	372.18	549.85	676.93	372.93	371.91	371.99	550.50	327.27	303.66	316.60
420	324.51	−436.9	38.99	324.55	514.85	650.64	325.36	324.26	324.35	516.57	276.20	250.79	264.72
RMSE**	****	631.97	236.97	0.0393	158.01	270.8	0.7049	0.206	0.2171	159.5	40.116	61.217	49.643

*Second virial coefficients are negative with units of cm^3/mol.
**Root mean square error between RK and the respective model for 18 temperatures between 250 and 420 K at 10° intervals.

for model 11. Figures 11a-d show that MCT-1 is overly conservative, eliminating only the "bad models" 1, 2, 4, and 5. The remaining models pass the MCT-1 while Table 7 shows that none but those containing the $T^{-3/2}$ term provide accurate $B(T)$. For real J-T coefficient data reduction to $B(T)$, it is thus preferable not to select a temperature model but rather use a literature $B(T)$ from a high temperature density measurement and integrate numerically Eq. 21 for (B/T). This procedure is generally used by J-T experimentalists, and Table 7 shows that they have little choice. The J-T flow experiment contains no adsorption errors, and if the single $B(T)$ is taken from density data above the critical temperature, the resultant $B(T)$ should be as accurate as the J-T coefficients because the PF are nearly unity as shown below.

Simulations with Random Errors. Only model 3 results will be considered in the remainder of this section for reasons outlined above. J-T coefficients measured to a precision of 0.1% or 1,000 ppm are considered excellent data whereas measurements of this derivative to 1% or 10,000 ppm are more commonplace, particularly in the older literature.

Table 8 contains the results of four simulations—two at the 1,000 ppm level and two at the 10,000 ppm level. For each error level, one simulation has a high mean and the other a low mean; additional statistical information is provided by Van Peursem (1991). Again, the random errors in μ_{JT} become systematic in $B(T)$ due to the assumption of a temperature form—(R-K form). Table 8 further shows the errors in $B(T)$ to be higher at higher temperatures, except for the first simulation. Propagation factors range from near 0.1 to 3.1 and so are much less than those for sonic speeds or density measurements. Table 8 implies that negative random errors damage $B(T)$ more than positive errors and whether the mean error is low or high is unimportant. Here, we multiply the (ΔB) at 1,000 ppm by ten for comparison to (ΔB) at 10,000 ppm for comparison of all four simulations. However, we are again drawing questionable conclusions. One conclusion is certain: Repetition of μ_{JT} data in the same laboratory with no systematic errors and using the correct temperature form can provide $B(T)$ differing up to about 15 cm^3/mol at 10,000 ppm RE. Reduction of the RE to 1,000 ppm provides $B(T)$ to a few cm^3/mol, which is usually acceptable.

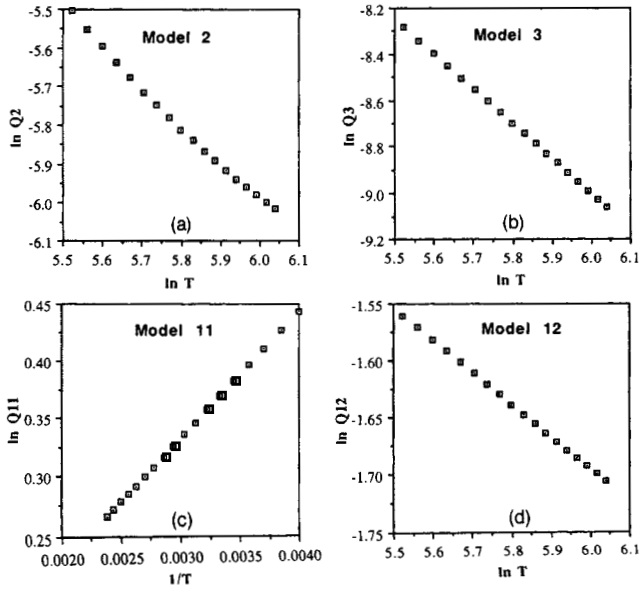

Figure 11. First-order model consistency test with error-free Joule-Thomson data.

Simulations with Systematic Errors. Fixed absolute errors (FAE) of 10,000 ppm or 1.41226×10^{-5} K/Pa were added (or subtracted) to each value of μ_{JT}(EF). The results are shown in Table 9. A positive error in μ_{JT} causes a negative error in $B(T)$ as seen by Eq. 21. The results for a negative error of 10,000 ppm are the same as in Table 9 but with a positive sign for all ΔB. Likewise, results at the 10,000 ppm level can be found by dividing the (ΔB) values of Table 9 by ten whereas the PF are unchanged.

Fixed fractional errors (FFE) of 10,000 ppm were added next to each value of μ_{JT}(EF). The results in Table 10 for a positive error again applies to a negative error by reversing the signs of all ΔB. Our PF is based upon fractional errors (Eq. 6) and so is unity here because $T^2[d(B/T)/dT]$ is the first virial coefficient of $\mu_{JT}C_p$ or $[-(\partial H/\partial T)_p]$. The corresponding PF were higher (~ 1.8) for sound speeds because both the first (γ^*) and second ($F(T)$) sonic virial coefficients are affected by a FFE and both sonic virial coefficients appear in the connecting identity, Eq. 18. Thus, FFE are more damaging to sound speeds whereas FAE are more damaging to J-T coefficients.

Adsorption errors were not simulated for J-T coefficients because they are not present in flow calorimetry.

Conclusions

Sound speeds

$B(T)$ can be obtained from precise $W^2(P,T)$ measurements

Table 8. Four Random Error Simulations of the Joule-Thomson Coefficient Experiment

Simulations at 1,000 ppm Level

		1(LPM)			2(HNM)		
T/K	RK	Model 3	PF	ΔB	Model 3	PF	ΔB
250	801.533	801.679	0.155	−0.125	801.729	0.218	−0.175
270	705.356	705.501	0.168	−0.118	705.715	0.471	−0.332
300	590.460	590.604	0.188	−0.111	591.014	0.881	−0.520
330	501.064	501.207	0.210	−0.105	501.769	1.331	−0.667
360	429.892	430.035	0.235	−0.101	430.717	1.822	−0.783
390	372.136	372.279	0.261	−0.097	373.059	2.359	−0.878
420	324.505	324.647	0.290	−0.094	325.509	2.945	−0.956
RMSE**	******	0.1098	******	*****	0.7049	******	******

Simulations at 10,000 ppm Level

		3(HPM)			4(LNM)		
T/K	RK	Model 3	PF	ΔB	Model 3	PF	ΔB
250	801.533	801.058	0.062	0.496	808.347	0.848	−6.793
270	705.356	704.243	0.161	1.139	712.861	1.060	−7.479
300	590.460	588.586	0.323	1.907	598.791	1.405	−8.298
330	501.064	498.598	0.500	2.504	510.037	1.783	−8.935
360	429.892	426.954	0.693	2.980	439.376	2.196	−9.442
390	372.136	368.815	0.904	3.366	382.035	2.648	−9.854
420	324.505	320.869	1.135	3.684	334.746	3.141	−10.193
RMSE**	******	2.6679	******	*****	9.1507	******	******

*Second virial coefficients are negative with units of cm^3/mol.
**Root mean square error between model 3 and R-K for 18 temperatures between 250 and 420 K at 10° intervals.

over a wide temperature range when a model consistency test (MCT) is used to prove that the assumed temperature form is consistent with the original data. Two MCT were developed here with the second test being highly selective for error-free data and for data with less than about 10 ppm random error. Both tests are of value for data between 10 and 50 ppm RE. However, above 50 ppm RE only the first test (MCT-1) is of value and then only to discard particularly poor temperature models.

Random errors propagate systematically into $B(T)$ because of the necessity of choosing a temperature form due to having a second-order differential equation as the connecting identity. A number of RE simulations have been shown to warn the reader against drawing conclusions from a single simulation. The combination of RE with temperature model selection leads to complex results. With the correct temperature model (RK), propagation factors range from 100 fold at 250 K to 30 fold at 420 K, but these values can vary by two to three times depending not on error level but upon the statistics of the particular random error generation, particularly the presence (or absence) of dominant outliers. We recommend that a future speed of sound investigation include three or four duplicate data sets for comparison with the present study.

Common systematic errors in sound speed experiments are likely to be unimportant to $B(T)$ because the PF range is from below unity to only two. Strong adsorption errors may be important but only at the 50 ppm level of Table 6. Actual adsorption errors are thought to be several orders of magnitude less and detectable by sonic experimentalists. However, adsorption errors generally cause $B(T)$ to be more negative similar to $B(T)$ from density measurements.

Random errors and the selection of a consistent temperature model appear to be the major factors affecting $B(T)$ from modern sound speed experiments. It is unlikely, however, that either can explain the large differences (60–100 cm^3/mol) between density measurements and the previously referenced sonic measurements of Ewing and coworkers. Because Ewing is systematically less negative at lower temperatures for the five C_4-

Table 9. Results with Positive Fixed Absolute Errors of 10,000 ppm for J-T Experiments*

T/K	RK	Model 3	PF	ΔB
250	801.533	819.80	4.19	−18.24
270	705.356	724.10	4.04	−18.72
300	590.460	609.78	3.84	−19.28
330	501.064	520.82	3.67	−19.72
360	429.892	450.01	3.53	−20.07
390	372.136	392.54	3.41	−20.36
420	324.505	345.14	3.30	−20.59
RMSE**	*****	20.235	******	******

*Second virial coefficients are negative with units of cm^3/mol.
**Root mean square error between model 3 and R-K for 18 temperatures between 250 and 420 K at 10° intervals.

Table 10. Results with Positive Fixed Fractional Errors of 10,000 ppm for J-T Experiments*

T/K	RK	Model 3	PF	ΔB
250	801.533	809.570	1.000	−8.016
270	705.356	712.436	1.000	−7.054
300	590.460	596.398	1.000	−5.905
330	501.064	506.113	1.000	−5.011
360	429.892	434.233	1.000	−4.299
390	372.136	375.903	1.000	−3.722
420	324.505	327.799	1.000	−3.246
RMSE**	*****	5.5026	******	******

*Second virial coefficients are negative with units of cm^3/mol.
**Root mean square error between model 3 and R-K for 18 temperatures between 250 and 420 K at 10° intervals.

C_5 alkanes, Table 5 indicates that this repetitive occurrence could only happen if Ewing consistently chose a "poor" temperature form inconsistent with his sonic data. While he did not use MCT as proposed here, Ewing did use model 11 (exponential) and also recalculated $W^2(P,T)$ from his final constants in model 11 as a consistency check. For *n*-butane (Ewing et al., 1988), three different semi-empirical models were used with resulting differences in $B(T)$ of less than ± 2 cm^3/mol from 250–320 K. These results and those of Goodwin and Moldover (1990) for a much higher reduced temperature of 0.9 are consistent with those of this study.

Excluding the possibility of much higher than imagined adsorption errors or some previously unrecognized systematic error in sound speeds, we must side with Ewing in ascribing the large $B(T)$ differences to adsorption in the density measurements at low reduced temperatures. As P-V-T experimentalists, we disclaim Ewing's references (for example, Das et al., 1973, for *n*-butane) to our correlations of alkane literature data with an original B-W-R/EOS covering a wide range of temperature and pressures, including the liquid. This EOS, which is infamous for providing too negative $B(T)$ at low reduced temperatures, was later modified by Starling to alleviate this problem. Measured $B(T)$ should be used to tune EOS but not the reverse; only in simulations, as explained previously, is it permissible to use an EOS because it need not mimic exactly the real world. Our present use of the RK/EOS which provides too positive $B(T)$ compared with real gases at low reduced temperatures, does not bias the present work in any way towards Ewing's side of the sonic/density controversy. We are presently measuring *n*-butane and neo-pentane in a P-V-T apparatus designed for polar gases and low reduced temperatures; adsorption to 10 ppm can be detected and corrected as in our steam measurements (Eubank et al.,1988). Our methanol densities (Kudchadker and Eubank, 1970) are uncorrected for adsorption but agree well in $B(T)$ with sonic derived values from Ewing's laboratory (Boyes et al., 1992b) from 323–473 K. That we are 194 cm^3/mol lower at 298 K is no doubt due to adsorption in our original P-V-T apparatus, which could not detect adsorption.

Even in the absence of adsorption, modern sound speed measurements are competitive with density for production of precise $B(T)$. While the PF are three to ten times higher for sonic data, random errors in density measurements cannot be reduced below about 100 ppm corresponding to roughly ± 0.2 cm^3/mol in $B(T)$. Sound speeds with RE of 10 ppm are thus more than competitive with densities measured to 100 ppm.

Joule-Thomson coefficients

J-T data should be integrated numerically to obtain $B(T)$ because of the major undetectable errors caused by assumption of the temperature model. Propagation factors are low (0.1 to 3.0 fold) for both random and systematic errors and, unlike sonic speeds, are generally highest at the highest temperatures. Taking a single $B(T)$ from density measurements at a supercritical temperature and integrating numerically with the μ_{JT} data down to lower temperatures is thus a good procedure. The major problem here is the high error levels present in most J-T data. If these can be substantially reduced, then J-T measurements can ultimately provide better $B(T)$ than either sound speeds or densities.

Acknowledgments

This research was funded by the National Science Foundation, grant CTS-9021129. Technical advice is acknowledged from Mr. Bruce Gammon and Dr. Kenneth Marsh, Thermodynamics Research Center, Texas A&M University, and from Prof. Chris Wormold, School of Chemistry, University of Bristol, UK. Technical discussions with Prof. Michael Ewing, Dr. A. R. H. Goodwin, Prof. Sam Colgate, and Prof. J. P. M. Trusler concerning their sound speed measurements are acknowledged. Finally, we thank Dr. Costa Tsonopoulos of Exxon R&E, who initially alerted us to the necessity of this project.

Notation

a = attraction parameter in the Redlich/Kwong EOS
b = repulsion parameter in the Redlich/Kwong EOS
B, $B(T)$ = density second virial coefficient, cm^3/mol
B_{EF} = error free second virial coefficient
B_{RK} = second virial coefficient for the Redlich/Kwong simulation model
ΔB = $(B - B_{RK})$
C, $C(T)$ = density third virial coefficient
C_p^* = isobaric ideal-gas-state heat capacity
C_v^* = isochoric ideal-gas-state heat capacity
F, $F(T)$ = speed of sound function $(\beta_a/2)$
G, $G(T)$ = Joule-Thomson function, $T^2\,[d(B/T)/dT]$
H = enthalpy
k_i = exponent on temperature in a single temperature term second virial coefficient model
M = molecular weight
n = repulsion interaction parameter in the Lennard-Jones potential (6,n)
n^+, n^- = number of positive (negative) RND in a RE simulation
P, $P(\rho,T)$ = pressure
P_c = critical pressure
Q_i = model consistency function
R = universal gas constant (83.1441 bar·cm^3/mol·K)
T = temperature, K
T_c = critical temperature
v = vapor; constant volume
V = molar volume
W = sound speed, m/s
W_{EF} = error-free sound speed
W_o = ideal gas sound speed
X = hypothetical variable
X_{EF} = error-free hypothetical variable
X_{FAE} = hypothetical variable with fixed absolute errors
X_{FFE} = hypothetical variable with fixed fractional errors
X_{RE} = hypothetical variable with random errors
Z = compressibility factor (PV/RT)

Greek letters

β_a = acoustic second virial coefficient, cm^3/mol
β_i = coefficients in various temperature models for $B(T)$
γ^* = ratio of ideal-gas-state heat capacities, C_p^*/C_v^*
γ_a = acoustic third virial coefficient, cm^3/bar^2·mol
δ_{FAE} = fixed absolute error scaling factor
δ_{FFE} = fixed fractional error scaling factor
δ_{RE} = random error scaling factor
μ_{JT} = Joule-Thomson coefficient, K/bar
ρ = molar density, cm^3/mol
σ = saturated property

Acronyms

EF = error free
EOS = equation of state
FAE = fixed absolute errors
FFE = fixed fractional errors
HNM = high negative mean
HPM = high positive mean
J-T = Joule-Thomson coefficient
LJ = Lennard-Jones potential

LNM = low negative mean
LPM = low positive mean
MCT = model consistency test
NBP = normal boiling point
PF,PF(T) = propagation factor
RE = random error
RK = Redlich/Kwong
RMSE = mean square error
RND = random number deviate

Literature Cited

Boyes, S. J., M. B. Ewing, and A. R. H. Goodwin, "Virial Coefficients for C_1-C_5 Alkanes from Speed of Sound Measurements," IUPAC Conf. on Chemical Thermodynamics, Snowbird, UT (1992a).

Boyes, S. J., M. B. Ewing, and A. R. H. Goodwin, "Heat Capacities and Second Virial Coefficients for Gaseous Methanol Determined from Speed-of-Sound Measurements at Temperatures between 280 K and 360 K and Pressures from 1.03 kPa to 80.5 kPa.," *J. Chem. Thermody.*, **34**, 1151 (1992b).

Chen, S. S., R. C., Wilhoit, and R. C. Zwolinski, "Ideal Gas Thermodynamic Properties and Isomerization of *n*-Butane and Isobutane," *J. Phys. Chem. Ref. Data*, **4**, 859 (1975).

Chao, Y.-P., "Simulation of Sonic Velocities of *n*-Butane in the Gas State for Determination of Second Virial Coefficients," MS Thesis, Texas A&M Univ., College Station (1990).

Das, T. R., C. O. Reed, and P. T. Eubank, "PVT Surface and Thermodynamic Properties of *n*-Butane," *J. Chem. Eng. Data*, **18**, 224 (1973).

Dymond, J. H., and E. B. Smith, *The Virial Coefficients of Pure Gases and Mixtures*, Clarendon Press, Oxford (1980).

Eubank, P. T., L. L. Joffrion, M. R. Patel, and W. Warowny, "Experimental Densities and Virial Coefficients for Steam from 348 to 498 K with Correction for Adsorption Effects," *J. Chem. Thermody.*, **20**, 1009 (1988).

Eubank, P. T., L. Yurttas, L. L. Joffrion, M. R. Patel, and W. Warowny, "Experimental Densities and Virial Coefficients for Steam from 348 to 498 K with Correction and Simulation of Adsorption Effects," *Properties of Water & Steam*, M. Pichal and O. Sifner, eds., Hemisphere, New York (1990).

Ewing, M. B., A. R. H. Goodwin, M. L. McGlashan, and J. P. M. Trusler, "Thermophysical Properties of Alkanes from Speeds of Sound Determined Using a Spherical Resonator: I. Apparatus, Acoustic Model, and Results for Dimethylpropane," *J. Chem. Thermody.*, **19**, 721 (1987).

Ewing, M. B., A. R. H. Goodwin, M. L. McGlashan, and J. P. M. Trusler, "Thermophysical Properties of Alkanes from Speeds of Sound Determined Using a Spherical Resonator: II. *n*-Butane," *J. Chem. Thermody.*, **20**, 243 (1988).

Ewing, M. B., A. R. H. Goodwin, M. L. McGlashan, and J. P. M. Trusler, "Thermophysical Properties of Alkanes from Speeds of Sound Determined Using a Spherical Resonator: III. *n*-Pentane," *J. Chem. Thermody.*, **21**, 867 (1989).

Ewing, M. B., A. R. H. Goodwin, and J. P. M. Trusler, "Thermophysical Properties of Alkanes from Speeds of Sound Determined Using a Spherical Resonator: IV. 2-Methyl-propane at Temperatures in the Range 252 K to 320 K and Pressures in the Range 5 kPa to 114 kPa," *J. Chem. Thermody.*, **23**, 1107 (1991).

Ewing, M. B., and A. R. H. Goodwin, "Thermophysical Properties of Alkanes from Speeds of Sound Determined Using a Spherical Resonator: V. Methylbutane," *J. Chem. Thermody.*, **24**, 301 (1992a).

Ewing, M. B., and A. R. H. Goodwin, "Speed of Sound, Perfect Gas Heat Capacities, and Acoustic Virial Coefficients for Methane Determined Using a Spherical Resonator at Temperatures Between 255 K and 300 K and Pressure in the Range 171 kPa to 7.1 MPa," *J. Chem. Thermody.*, **24**, 1257 (1992b).

Goodwin, A. R. H., and M. R. Moldover, "Thermophysical Properties of Gaseous Refrigerants from Speed of Sound Measurements: I. Apparatus, Model, and Results for 1,1,1,2-Tetrafluoroethane R134a," *J. Chem. Phys.*, **93**, 2741 (1990).

Hall, K. R., and P. T. Eubank, "Burnett-Isochoric Coupled Data with Application to Adsorbing Gases," *Physica*, **61**, 346 (1972).

Holldorff, H., and H. Knapp, "Vapor Pressures of n-Butane, Dimethyl Ether, Methyl Chloride, Methanol and the Vapor-Liquid Equilibrium of Dimethyl Ether-Methanol," *Fluid Phase Equilibr.*, **40**, 113 (1988).

Kennedy, E. R., B. H. Sage, and W. N. Lacey, "Phase Equilibria in Hydrocarbon Systems," *Ind. Eng. Chem.*, **28**, 718 (1936).

Kerns, W. J., and P. T. Eubank, "Adsorbtion and Molecular Association with the Burnett Apparatus," *AIChE J.*, **19**, 711 (1973).

Kudchadker, A. P., and P. T. Eubank, "The Second Virial Coefficient of Methanol," *J. Chem. Eng. Data*, **15**, 7 (1970).

Maitland, G. C., M. Rigby, E. B. Smith, and W. A. Wakeham, *Intermolecular Forces: Their Origin and Determination*, Clarendon Press, Oxford, p. 130 (1981).

Mansoorian, H., K. R. Hall, J. C. Holste, and P. T. Eubank, "The Density of Gaseous Ethane and of Fluid Methyl Chloride, and the Vapor Pressure of Methyl Chloride," *J. Chem. Thermody.*, **13**, 1001 (1981).

Mehl, J. B., and M. R. Moldover, "Precondensation Phenomena in Acoustic Measurements," *J. Chem. Phys.*, **77**(1), 455 (1982).

Smith, J. M., and H. C. Van Ness, *Introduction to Chemical Engineering Thermodynamics*, 4th ed., McGraw-Hill, New York, p. 109 (1987).

Trusler, J. P. M., and M. Zarari, "The Speed of Sound and Derived Thermodynamic Properties of Methane at Temperature between 275 K and 3375 K and Pressures up to 10 MPa," *J. Chem. Thermody.*, **24**, 973 (1992a).

Trusler, J. P. M., and M. Zarari, "Gaseous Equations of State Determined from the Speed of Sound," IUPAC Conference on Chemical Thermodynamics, Snowbird, UT (1992b).

Van Dael, W., "Thermodynamic Properties and the Velocity of Sound," *Experimental Thermodynamics*, Vol. 2, B. Le Neidre and B. Vodar, eds., Butterworths, London, p. 542 (1975).

Van Peursem, D. J., "Simulation Study on Error Propagation Effects when Determining Second Virial Coefficients from the Speed-of-Sound or the Joule-Thomson Experiment," MS Thesis in Chemical Engineering, Texas A&M Univ., College Station (1991).

Manuscript received June 21, 1993, and revision received Nov. 29, 1993.